

PAPER

Effect of temperature on photoresponse properties of solar-blind Schottky barrier diode photodetector based on single crystal Ga<sub>2</sub>O<sub>3</sub>\*

Recent citations

- [Temperature-Dependent Crystallization of Ga<sub>2</sub>O<sub>3</sub> for Ultraviolet Photodetectors](#)  
Jinjie Wu *et al*

To cite this article: Chao Yang *et al* 2019 *Chinese Phys. B* **28** 048502

View the [article online](#) for updates and enhancements.

# Effect of temperature on photoresponse properties of solar-blind Schottky barrier diode photodetector based on single crystal Ga<sub>2</sub>O<sub>3</sub>\*

Chao Yang(杨超)<sup>1</sup>, Hongwei Liang(梁红伟)<sup>1,†</sup>, Zhenzhong Zhang(张振中)<sup>2</sup>, Xiaochuan Xia(夏晓川)<sup>1</sup>, Heqiu Zhang(张贺秋)<sup>1</sup>, Rensheng Shen(申人升)<sup>1</sup>, Yingmin Luo(骆英民)<sup>1</sup>, and Guotong Du(杜国同)<sup>1</sup>

<sup>1</sup>School of Microelectronics, Dalian University of Technology, Dalian 116024, China

<sup>2</sup>State Key Laboratory of Luminescence and Applications, Changchun Institute of Optics, Fine Mechanics and Physics, Chinese Academy of Sciences, Changchun 130033, China

(Received 20 November 2018; revised manuscript received 5 January 2019; published online 5 March 2019)

A solar-blind photodetector is fabricated on single crystal Ga<sub>2</sub>O<sub>3</sub> based on vertical structure Schottky barrier diode. A Cu Schottky contact electrode is prepared in a honeycomb porous structure to increase the ultraviolet (UV) transmittance. The quantum efficiency is about 400% at 42 V. The Ga<sub>2</sub>O<sub>3</sub> photodetector shows a sharp cutoff wavelength at 259 nm with high solar-blind/visible (= 3213) and solar-blind/UV (= 834) rejection ratio. Time-resolved photoresponse of the photodetector is investigated at 253-nm illumination from room temperature (RT) to 85.8 °C. The photodetector maintains a high reversibility and response speed, even at high temperatures.

**Keywords:** Ga<sub>2</sub>O<sub>3</sub> single crystal, solar-blind, photodetector, high temperature

**PACS:** 85.60.Gz, 95.85.Mt, 85.30.Kk, 73.30.+y

**DOI:** 10.1088/1674-1056/28/4/048502

## 1. Introduction

A solar-blind photodetector is used in the detection of photon signal shorter than 280 nm and scarcely responds to the wavelength above 280 nm. Owing to the strong absorption by the ozone layer, the radiation in the range 200 nm–280 nm emitted by the sun cannot reach the Earth's surface.<sup>[1,2]</sup> Therefore, 'zero-background noise' is a prominent advantage for the application of solar-blind wavelength in many communication fields. The solar-blind photodetector is now widely applied in missile warning, corona electrical discharge, fire alarms, ozone monitoring, under water and space communication, and so on.<sup>[3–6]</sup>

Various wide band gap semiconductors have been investigated to fabricate solar-blind photodetectors, such as  $\beta$ -Ga<sub>2</sub>O<sub>3</sub>, Al<sub>x</sub>Ga<sub>1-x</sub>N, Mg<sub>x</sub>Zn<sub>1-x</sub>O. High Al and Mg composition is, respectively, necessary to modulate the band gap of AlGaN and MgZnO and keeps the photodetector response range in solar-blind wavelength. However, the crystal quality of AlGaN films deteriorates rapidly<sup>[1,7–9]</sup> and the MgZnO appears phase segregation<sup>[10,11]</sup> as the Al or Mg composition increases.  $\beta$ -Ga<sub>2</sub>O<sub>3</sub> is one of the most suitable materials for solar-blind photodetection because its band gap ( $E_g$ ) is about 4.9 eV and locates at the center position of the solar-blind wavelength without the need of composition modulation. Ga<sub>2</sub>O<sub>3</sub> solar-blind photodetectors are mainly fabricated

on nanostructure, thin films, and single crystal. Solar-blind photodetectors based on Ga<sub>2</sub>O<sub>3</sub> nanostructure are characterized by simple growth and high internal gains.<sup>[12,13]</sup> Nevertheless, the solar-blind Ga<sub>2</sub>O<sub>3</sub> photodetector with large size of detect area or even capability of imaging is desired in many application fields.<sup>[6,14,15]</sup> Large size and high quality Ga<sub>2</sub>O<sub>3</sub> single crystals can be achieved through conventional methods such as floating zone (FZ),<sup>[16]</sup> edge-defined film-fed growth (EFG),<sup>[17]</sup> and Czochralski (CZ)<sup>[18]</sup> methods. Moreover, high quality Ga<sub>2</sub>O<sub>3</sub> single crystals can reduce the defects density to a very low level and lower the effect of persistent photoconductivity, and thus increase the device response speed.

A junction-type Ga<sub>2</sub>O<sub>3</sub> photodetector, compared with photoconductive type, presents a higher response speed at room temperature (RT). The photoresponse properties of photodetector at higher temperature are even more important in applications such as flame detection. However, few studies of the properties of junction-type Ga<sub>2</sub>O<sub>3</sub> photodetector at high temperature have been published. Among the various kinds of junction-type Ga<sub>2</sub>O<sub>3</sub> photodetector, a relatively simple preparation process is required for Schottky barrier diode (SBD) photodetector. In this work, the current–voltage ( $I$ – $V$ ) characteristics, response speed, and solar-blind selectivity of Ga<sub>2</sub>O<sub>3</sub> SBD solar-blind photodetector are investigated. Meanwhile, a Cu Schottky electrode with honeycomb porous structure is adopted to the fabrication of solar-blind photodetector. The

\*Project supported by National Key Research and Development Plan of China (Grant Nos. 2016YFB0400600 and 2016YFB0400601), the National Natural Science Foundation of China (Grant Nos. 61574026, 11675198, 61774072, and 11405017), the Natural Science Foundation of Liaoning Province, China (Grant Nos. 201602453 and 201602176), China Postdoctoral Science Foundation Funded Project (Grant No. 2016M591434), and the Dalian Science and Technology Innovation Fund (Grant No. 2018J12GX060).

†Corresponding author. E-mail: [hwliang@dlut.edu.cn](mailto:hwliang@dlut.edu.cn)

photodetector presents good rectifying properties at RT and clear photoresponse to the ultraviolet shorter than 259 nm and maintains a high reversibility and response speed, even at 85.8 °C.

## 2. Experimental details

The commercial ( $\bar{2}01$ )-orient  $\beta$ -Ga<sub>2</sub>O<sub>3</sub> substrate with 600- $\mu$ m thickness is used to fabricate the SBD photodetector by cutting along the [010] and [102] orientation into 5 mm  $\times$  5 mm pieces. The unintentional doped Ga<sub>2</sub>O<sub>3</sub> crystal is n-type with a carrier concentration of about  $10^{17}$  cm<sup>-3</sup>. The sample is degreased using methanol (5 min)/acetone (5 min)/methanol (5 min)/deionized water (5 min), successively. Then, the samples are etched in the solution with H<sub>2</sub>SO<sub>4</sub>:H<sub>2</sub>O<sub>2</sub>:H<sub>2</sub>O = 4:1:1 for 5 min. Finally, the samples are dipped in 90-°C deionized water.

The metal deposition is performed by vacuum thermal evaporation method. A Ti/Au (20 nm/200 nm) Ohmic contact with 4 mm  $\times$  4 mm is first deposited on the back side of the substrate and is subsequently thermally annealed at 450 °C in nitrogen for 3 min. Cu is used to prepare Schottky contact because it can form similar effective barrier height to that prepared with Au,<sup>[19,20]</sup> which is also proven in this work. Moreover, the adhesion property of Cu electrode is much better than Ni and Au in our experiments. The 200-nm Cu electrode is deposited on the top surface of the Ga<sub>2</sub>O<sub>3</sub> substrate. Cu Schottky electrodes with a diameter of 0.6-mm are formed to investigate the effect of annealing temperature on the electrical properties of Cu/Ga<sub>2</sub>O<sub>3</sub> SBD. Samples are annealed at 100 °C/200 °C/300 °C in nitrogen for 5 min. The  $I$ - $V$  characteristics of Cu/Ga<sub>2</sub>O<sub>3</sub> SBD obtained from the samples annealed at different temperature show that relatively better rectifying properties can be achieved after being annealed at 200 °C. Consequently, the Cu Schottky electrode of Ga<sub>2</sub>O<sub>3</sub> solar-blind photodetector is annealed at 200 °C in nitrogen for 5 min. The Schottky electrode of the photodetector is prepared using standard photolithography and lift-off techniques. The electrode is designed in honeycomb porous structure with diameter of 2.8 mm. Any three adjacent holes can be grouped into an equilateral triangle. The diameter of the holes and spacing between them are 40  $\mu$ m in this experiment and the effect of the size on the photoresponse properties will be investigated in future experiments. The schematic structure of the photodetector is shown in the inset of Fig. 1(a).

The  $I$ - $V$  characteristics for the SBD are measured using Keithley 4200-SCS semiconductor characterization system. Time-resolved photocurrent response spectra are conducted under 253-nm light with Keithley 4200-SCS semiconductor characterization system. The photoresponse spec-

tra of the photodetectors are measured in an SPEX scanning monochromator employing a 150-W Xe lamp as the illumination source. The responsivity spectrum is obtained by measuring the photocurrent (calibrated with a standard Si photodiode) under the illumination of an Xe lamp spectrum from 200 nm to 500 nm using a scanning monochromator.

## 3. Results and discussion

The forward and reverse  $I$ - $V$  characteristics of the Cu/Ga<sub>2</sub>O<sub>3</sub> SBD annealed at different temperatures are shown in Fig. 1. The forward current is linear in the semilogarithmic scale at low forward bias voltages as shown in Fig. 1(a). The dominant current transport mechanism can be determined by comparing the thermal energy  $KT$  with  $E_{00}$  ( $= (q\hbar/2)\sqrt{N/m^*\epsilon_S}$ ). When  $KT \gg E_{00}$ , thermionic emission is the dominant transport mechanism.<sup>[21]</sup> Considering the effect of series resistance  $R_s$ , the diode equations can be written as Eq. (1):<sup>[22,23]</sup>

$$I = I_s \exp\left(\frac{q(V - IR_s)}{nKT}\right) \left(1 - \exp\left(-\frac{q(V - IR_s)}{KT}\right)\right), \quad (1)$$

where  $I_s = A^{**}T^2 \exp(-q\phi_b/kT)$ .  $I$ ,  $I_s$ ,  $V$ ,  $K$ ,  $q$ ,  $n$ ,  $A^{**}$ ,  $\phi_b$ , and  $T$  is current, saturation current density, applied forward bias voltage, Boltzmann constant, elementary charge, ideality factor, effective Richardson constant, barrier height, and temperature, respectively. The effective Richardson constant  $A^{**}$  is calculated to be  $41.04 \text{ A}\cdot\text{cm}^{-2}\cdot\text{K}^{-2}$ <sup>[24]</sup> at RT, using electron effective mass  $m^* = 0.342 m_0$ ,<sup>[25]</sup> and free electron Richardson constant  $A^* = 120 \text{ A}\cdot\text{cm}^{-2}\cdot\text{K}^{-2}$ . Fitting this model to the linear range of the semi-log plot of  $I$  versus  $V$ , the change trend of  $\phi_b$  and  $n$  of all the samples annealed at different temperatures is shown in Fig. 1(c). The sample without annealing (w/o ann.) shows a relatively lower Schottky barrier height. As the annealing temperature increases, the barrier height increases while the ideality factor decreases first and then reaches a minimum (1.145) at 200 °C. When the annealing temperature increases further, the ideality factor increases slightly. The ideality factor results indicate the Cu/Ga<sub>2</sub>O<sub>3</sub> Schottky contact is closest to thermionic emission model after annealed at 200 °C. Reverse  $I$ - $V$  characteristics are shown in Fig. 1(b). The reverse current of the sample without annealing increases dramatically at low bias and shows poor rectifying properties. The current reduces by over two orders of magnitude after being annealed at 100 °C and reaches 10 nA at -48 V. The rectifying properties are improved and a current of 10 nA is obtained at a higher voltage (69 V) after being annealed at 200 °C. The reverse current increases slightly after annealed at 300 °C.

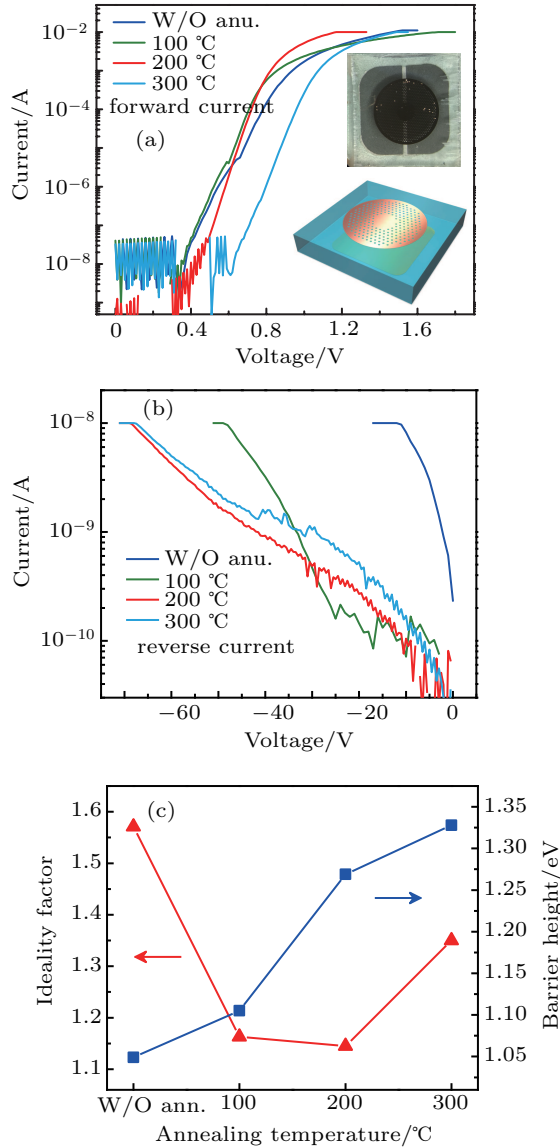


**Fig. 1.** The  $I$ - $V$  characteristics of the Cu/Ga<sub>2</sub>O<sub>3</sub> SBD annealed at different temperatures: (a) forward  $I$ - $V$  curves (the inset is the top view and schematic structure of the photodetector), (b) reverse  $I$ - $V$  curves, and (c) the ideality factor and barrier height.

Based on these results, the Schottky contact electrode of the photodetector is annealed in nitrogen at 200 °C for 5 min. The photoresponse spectra of the photodetector are measured at various reverse bias range from 0 V to 42 V. The responsivity of the photodetector can be calculated by Eq. (2):<sup>[26]</sup>

$$R_{\lambda} = \frac{I_{\text{photo}} - I_{\text{dark}}}{S \times P}, \quad (2)$$

where  $R_{\lambda}$  is the responsivity of the photodetector,  $I_{\text{photo}}$  is the photo current,  $I_{\text{dark}}$  is the dark current,  $S$  is the effective illuminated area, and  $P$  is the light intensity. The photoresponse spectra measured at 0 V and 42 V are shown in Fig. 2(a). An obvious response can be detected at solar-blind wavelength when zero bias voltage is applied, which proves that the device can be used as a self-powered solar-blind photodetector. The photocurrent at a 0 V bias is the result of the photovoltaic

effect. When the reverse bias is elevated to 42 V, the maximum responsivity is about 0.8 A/W. Quantum efficiency  $\eta$  is a function of  $R_{\lambda}$  as Eq. (3):<sup>[21,27]</sup>

$$\eta = \frac{hcR_{\lambda}}{e\lambda}, \quad (3)$$

where  $h$  is Planck's constant,  $c$  is the velocity of light,  $e$  is the basic electron charge, and  $\lambda$  is the incident light wavelength. The quantum efficiency exceeds 100% when the bias is larger than 36 V and reaches 400% at 42 V, which benefits from the honeycomb porous structural Schottky electrode. Although the UV photons are blocked by the region covered with Cu, the area of enhanced electric field in the depletion layer is beyond the edge of the Schottky electrode and forms ring area in the exposed holes to collect the photogenerated carriers. Highly symmetric electrode structure can reduce the concentration of electric field in some large curvature area. The maximum of responsivity and quantum efficiency of the photodetector at each bias are extracted out and the relation between the maximum value and reverse bias voltage is shown in Fig. 2(b). As the reverse bias increases, the responsivity increases gradually in the low bias range and then increases dramatically when the bias exceeds 35 V. The increased responsivity in low bias range can be attribute to the widening ring area with enhanced electric field as the reverse bias increases according to the simulation results (not shown here). The dramatically increased responsivity in high bias range is also analyzed in another report,<sup>[27]</sup> which is attributed to avalanche multiplication mechanism. The positive temperature coefficient of the breakdown voltage is recognized as the criterion to determinate avalanche mechanism.<sup>[13,21,28,29]</sup> However, no obviously positive shift of breakdown voltage is observed in the reverse dark current as the temperature increases as shown in Fig. 3(b), which indicates the response process involved other unknown gain mechanism. A further investigation will be required to obtain a better understanding of this mechanism. The cutoff wavelength and the rejection ratio are two important parameters to characterize the selectivity of solar-blind photodetector. The cutoff wavelength is defined as the ratio between the position of maximum responsivity and the natural constant ( $e \approx 2.718$ ). The cutoff wavelength of the photodetector is limited to 259 nm which demonstrates an excellent solar-blind selectivity. The solar-blind/visible (= 3213) and solar-blind/UV (= 834) rejection ratios are calculated from the ratio of responsivity at peak to 400 nm and peak to 280 nm, both of which indicate the photodetector scarcely responds to the light out of solar-blind range. A comparison among the reported solar-blind photodetectors<sup>[30-32]</sup> based on single crystal Ga<sub>2</sub>O<sub>3</sub> is summarized in Table 1 to analyze the effect of electrode on the photoresponse properties. A uniform semi-transparent electrode with a large area is adopted in the first two reports, both

of which show clear response to the light close to and even above 280 nm. This phenomenon can be attributed to the internal photoemission.<sup>[21]</sup> In this process, electrons in the thin electrode can surmount the Schottky barrier and be collected

by the semiconductor due to the excitation of smaller energy photon ( $q\phi_b < hc/\lambda < E_g$ ). While the response range of photodetector can be limited to solar-blind wavelength by a thicker electrode with interdigitated or honeycomb porous structure.

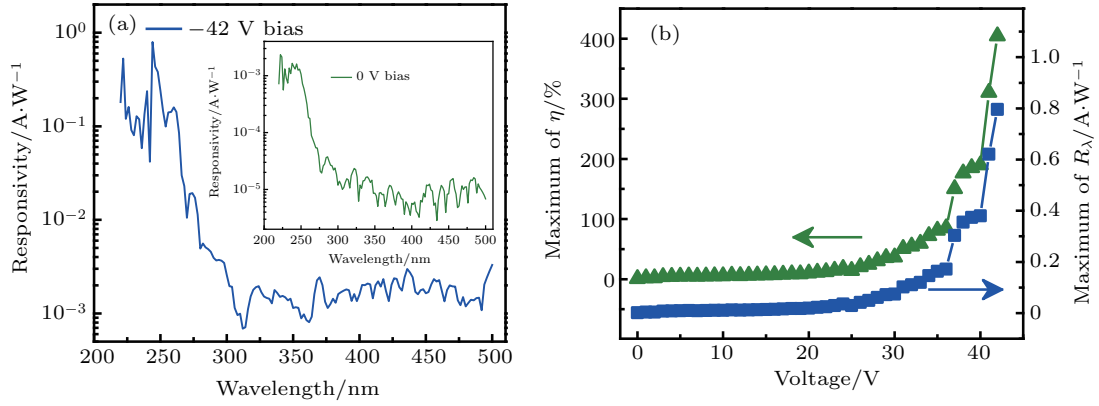


**Fig. 2.** Photoresponse characteristics for the photodetector: (a) responsivity of the detector measured under 0-V and 42-V biases, and (b) the relation between the reverse bias and the maximum of responsivity and quantum efficiency.

**Table 1.** Comparison of the photoresponse parameters among the single crystal Ga<sub>2</sub>O<sub>3</sub>-based photodetectors.

Structure of device	Electrode materials	Cutoff wavelength/nm	Ref.
Vertical Schottky	PEDOT-PSS	300	[30]
Vertical Schottky	Au	—	[31]
Interdigitated electrodes	Ti/Au	260	[32]
Vertical Schottky	Cu	259	this work

The  $I$ - $V$  characteristics of the photodetector is measured from RT to 85.8 °C, as shown in Fig. 3. Figure 3(a) shows the forward temperature-dependent  $I$ - $V$  characteristics of the photodetector. The ideality factor and barrier height are fitted based on the linear parts in the semilogarithmic scale, and are shown in Fig. 3(c). Both the ideality factor and the barrier height are almost a constant (1.05 and 1.20) at RT and higher temperatures, which is also mentioned in other reports.<sup>[33,34]</sup> An increase of the reverse dark current and a lowering of the reverse photo current with elevated temperature are observed in Fig. 3(b). The reason for the increase of dark current can be explained with Eq. (1), which can be written as a form of Eq. (4) under higher reverse bias:

$$I = I_s \exp\left(\frac{qV}{nKT}\right) \left(-\exp\left(-\frac{qV}{KT}\right)\right) = -A^{**} T^2 \exp\left(\frac{-(n-1)qV - nq\phi_b}{nKT}\right). \quad (4)$$

The reverse dark current monotonically increases with the elevated temperature. The reason for this lowering of photo current can be attributed to the comprehensive factors of enhanced carrier recombination,<sup>[35]</sup> stronger lattice scattering,<sup>[36]</sup> and the narrowing of depletion width  $W_D$  at high temperatures. The depletion width  $W_D$  can be written by Eq. (5)<sup>[21]</sup>

$$W_D = \sqrt{\frac{2\epsilon_s}{qN_D} \left(\psi_{bi} - V - \frac{KT}{q}\right)}, \quad (5)$$

where the  $\epsilon_s$  is dielectric permittivity,  $N_D$  is doping concentration, and  $\psi_{bi}$  is built-in potential. The first<sup>[33]</sup> and third terms in the parentheses decreases as the temperature increases, which weakens the separation of photogenerated electron-hole pairs.

The time-resolved photoresponse of the photodetector at different temperatures is carried out under 253-nm illumination by on/off switching. Ten cycles of on/off state current under  $-5$ -V and  $-10$ -V biases are shown in Figs. 4(a) and 4(b), respectively. Although a slight fluctuation of photocurrent is measured at  $-5$  V, the photodetector shows a high response speed—especially in the decay edge. When the reverse bias is set to  $-10$  V, the 10-periods photocurrent is stabilized at around 500 nA. As the temperature increases, the photocurrent shows almost no fluctuation. This proves the high reversibility and high reproducibility of the photodetector. Both the rise time curve and decay time curve can be fitted with a second-order exponential formula<sup>[37,38]</sup>

$$I = I_0 + A e^{-t/\tau_1} + B e^{-t/\tau_2}, \quad (6)$$

where  $I_0$  is the steady state photocurrent,  $t$  is the time,  $A$  and  $B$  are constants,  $\tau_1$  and  $\tau_2$  are two relaxation time constants corresponding to a fast-response component and a slow-response component. The constant  $\tau_1$  is related to the rapid change of



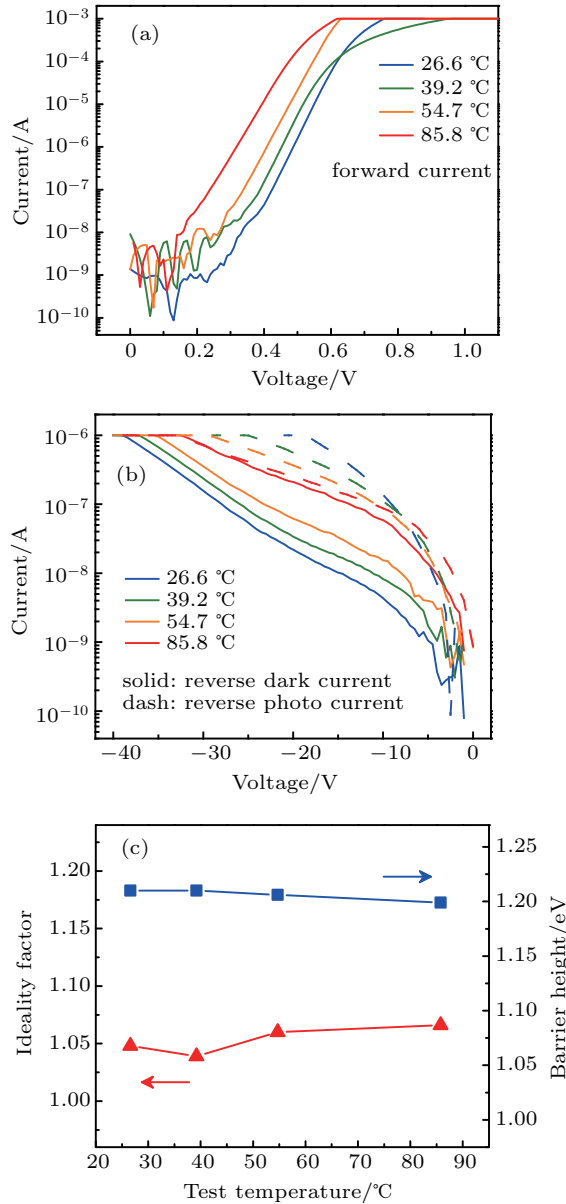


**Fig. 3.** The  $I$ - $V$  characteristics of the photodetector measured at different temperatures: (a) forward  $I$ - $V$  curves, (b) reverse  $I$ - $V$  curves under dark and illumination, and (c) the ideality factor and barrier height.

**Table 2.** The rise time constant  $\tau_r$  and decay time constant  $\tau_d$  at different temperatures at  $-10$ -V bias.

Test temperature/°C	26.6	39.2	54.7	85.8
$\tau_{r1}/\tau_{r2}$ constant/s	0.407/2.704	0.659/3.630	0.668/3.463	0.683/2.736
$\tau_d$ constant/s	0.133	0.163	0.097	0.186

#### 4. Conclusion

A vertical structural SBD solar-blind photodetector is fabricated on a single crystal  $\text{Ga}_2\text{O}_3$ . The effect of annealing temperature on  $\text{Cu}/\text{Ga}_2\text{O}_3$  Schottky contact properties is investigated and the Schottky electrode of the photodetector is annealed at  $200^\circ\text{C}$  in nitrogen for 5 min. The quantum efficiency of the photodetector can reach 400% at 42 V. High solar-blind selectivity of the photodetector is demonstrated by a sharp cutoff wavelength at 259 nm with high solar-blind/visible

the carrier concentration when the UV light is turned on/off, and  $\tau_2$  is related to carrier trapping and releases due to the oxygen vacancy defects.<sup>[39,40]</sup> The sharp decay edge results in two equal relaxation time constants, which means the formula is simplified to be  $I = I_0 + Ae^{-t/\tau_d}$ . The relaxation time constants are fitted based on time-resolved photocurrent plots at different temperatures under  $-10$ -V bias, as shown in Table 2. Both the rise time and decay time constant show almost no change as the temperature increases, which indicates a stable response speed of the photodetector at elevated temperature.

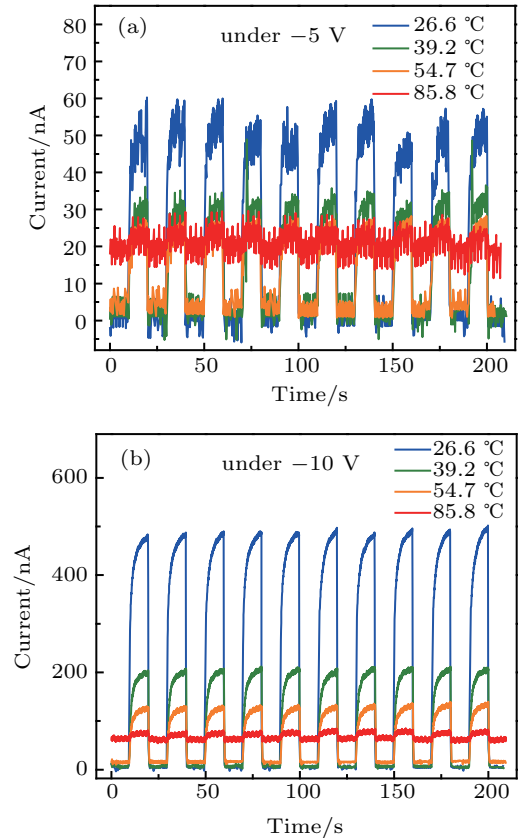


**Fig. 4.** Time-resolved characteristics of the solar-blind  $\text{Cu}/\text{Ga}_2\text{O}_3$  SBD photodetector measured at: (a)  $-5$  V and (b)  $-10$  V.

(= 3213) and solar-blind/UV (= 834) rejection ratio. Both the quantum efficiency and sharp cutoff wavelength benefit from the honeycomb porous structure Schottky electrode. The  $I$ - $V$  characteristics and time-resolved photoresponse of the photodetector are investigated at 253-nm illumination from RT to  $85.8^\circ\text{C}$ . Both of the ideality factor and barrier height are almost constant (1.05 and 1.20) at RT and higher temperatures. Although the elevated temperature leads to an increased dark current and decreased photocurrent, the photodetector main-

tains a high reversibility and response speed — even at high temperatures.

## References

- [1] Sang L, Liao M and Sumiya M 2013 *Sensors* **13** 10482
- [2] Razeghi M and Rogalski A 1996 *J. Appl. Phys.* **79** 7433
- [3] Razeghi M 2002 *Proc. IEEE* **90** 1006
- [4] Monroy E, Omnès F and Calle F 2003 *Semicond. Sci. Technol.* **18** R33
- [5] Xu Z Y and Sadler B M 2008 *IEEE Commun. Mag.* **46** 67
- [6] Li J, Zhou Y, Yi X, Zhang M, Chen X, Cui M and Yan F 2017 *Curr. Opt. Photon.* **1** 196
- [7] Walker D, Kumar V, Mi K, Sandvik P, Kung P, Zhang X H and Razeghi M 2000 *Appl. Phys. Lett.* **76** 403
- [8] Tut T, Gokkavas M, Inal A and Ozbay E 2007 *Appl. Phys. Lett.* **90** 163506
- [9] Parish G, Keller S, Kozodoy P, Ibbetson J P, March, H, Fini P T, Fleischer S B, DenBaars S P, Mishra U K and Tarsa E J 1999 *Appl. Phys. Lett.* **75** 247
- [10] Fan M M, Liu K W, Chen X, Wang X, Zhang Z Z, Li B H and Shen D Z 2015 *ACS Appl. Mater. Interfaces* **7** 20600
- [11] Wang L K, Ju Z G, Zhang J Y, Zheng J, Shen D Z, Yao B, Zhao D X, Zhang Z Z, Li B H and Shan C X 2009 *Appl. Phys. Lett.* **95** 131113
- [12] Zhao B, Wang F, Chen H, Zheng L, Su L, Zhao D and Fang X 2017 *Adv. Funct. Mater.* **27** 1700264
- [13] Zhao B, Wang F, Chen H, Wang Y, Jiang M, Fang X and Zhao D 2015 *Nano Lett.* **15** 3988
- [14] Chen Y C, Lu Y J, Lin C N, Tian Y Z, Gao C J, Dong L and Shan C X 2018 *J. Mater. Chem. C* **6** 5727
- [15] El-Shimy M A and Hranilovic S 2015 *J. Lightwave Technol.* **33** 2246
- [16] Ueda N, Hosono H, Waseda R and Kawazoe H 1997 *Appl. Phys. Lett.* **70** 3561
- [17] Aida H, Nishiguchi K, Takeda H, Aota N, Sunakawa K and Yaguchi Y 2008 *Jpn. J. Appl. Phys.* **47** 8506
- [18] Tomm Y, Reiche P, Klimm D and Fukuda T 2000 *J. Crystal Growth* **220** 510
- [19] Mohamed M, Irmscher K, Janowitz C, Galazka Z, Manzke R and Fornari R 2012 *Appl. Phys. Lett.* **101** 132106
- [20] Splith D, Muller S, Schmidt F, von Wenckstern H, van Rensburg J J, Meyer W E and Grundmann M 2014 *Phys. Status Solidi A* **211** 40
- [21] Sze S M and Ng K K 2007 *Phys. Semiconductor Devices*, 3rd edn. (Hoboken: John Wiley & Sons) pp. 165, 154–158, 681
- [22] Rhoderick E H and Williams R H 1988 *Metal-semiconductor Contacts*, 2nd edn. (Oxford: Clarendon) p. 99
- [23] Schroder D K 2006 *Semicond. Material Device Characterization*, 3rd edn. (Hoboken: John Wiley & Sons) p. 190
- [24] Sasaki K, Higashiwaki M, Kuramata A, Masui T and Yamakoshi S 2013 *IEEE Electron Dev. Lett.* **34** 493
- [25] He H, Orlando R, Blanco M A, Pandey R, Amzallag E, Baraille I and Rérat M 2006 *Phys. Rev. B* **74** 195123
- [26] Kong W Y, Wu G A, Wang K Y, Zhang T F, Zou Y F, Wang D D and Luo L B 2016 *Adv. Mater.* **28** 10725
- [27] Hu G C, Shan C X, Zhang N, Jiang M M, Wang S P and Shen D Z 2015 *Opt. Express* **23** 13554
- [28] Chen X, Xu Y, Zhou D, Yang S, Ren F F, Lu H, Tang K, Gu S, Zhang R, Zheng Y and Ye J 2017 *ACS Appl. Mater. Interfaces* **9** 36997
- [29] Mahmoud W E 2016 *Sol. Energy Mater. Sol. Cells* **152** 65
- [30] Oshima T, Okuno T, Arai N, Suzuki N, Hino H and Fujita S 2009 *Jpn. J. Appl. Phys.* **48** 011605
- [31] Suzuki R, Nakagomi S, Kokubun Y, Arai N and Ohira S 2009 *Appl. Phys. Lett.* **94** 222102
- [32] Mu W X, Jia Z T, Yin Y R, Hu Q Q, Zhang J, Feng Q, Hao Y and Tao X T 2017 *Crystengcomm* **19** 5122
- [33] Higashiwaki M, Konishi K, Sasaki K, Goto K, Nomura K, Thieu Q T, Togashi R, Murakami H, Kumagai Y, Monemar B, Koukitu A, Kuramata A and Yamakoshi S 2016 *Appl. Phys. Lett.* **108** 133503
- [34] Jayawardena A, Ahyi A C and Dhar S 2016 *Semicond. Sci. Technol.* **31** 115002
- [35] Xie F, Lu H, Chen D, Ji X, Yan F, Zhang R, Zheng Y, Li L and Zhou J 2012 *IEEE Sens. J.* **12** 2086
- [36] Li G, Zhang J and Hou X 2014 *Sens. Actuator A-Phys.* **209** 149
- [37] Reemts J and Kittel A 2007 *J. Appl. Phys.* **101** 013709
- [38] Liu N, Fang G, Zeng W, Zhou H, Cheng F, Zheng Q, Yuan L, Zou X and Zhao X 2010 *ACS Appl. Mater. Interfaces* **2** 1973
- [39] Juan Y M, Chang S J, Hsueh H T, Wang S H, Weng W Y, Cheng T C and Wu C L 2015 *RSC Adv.* **5** 84776
- [40] Rafique S, Han L and Zhao H 2017 *Phys. Status Solidi A* **214** 1700063